Published online 25 December 2013 *Nucleic Acids Research, 2014, Vol. 42, No. 6* ***3821–3832***
doi:10.1093/nar/gkt1316

Single molecule analysis of *Thermus thermophilus* SSB protein dynamics on single-stranded DNA

Jichuan Zhang[1,2], Ruobo Zhou[1], Jin Inoue[3], Tsutomu Mikawa[3] and Taekjip Ha[1,4,*]

[1]Department of Physics and Center for the Physics of Living Cells, University of Illinois, Urbana, IL 61801, USA, [2]Department of Materials Science and Engineering, University of Illinois, Urbana, IL 61801, USA, [3]RIKEN, Cellular and Molecular Biology Unit, 2-1 Hirosawa, Wako, Saitama 351-0198, Japan and [4]Howard Hughes Medical Institute, University of Illinois, Urbana, IL 61801, USA

Received June 27, 2013; Revised October 31, 2013; Accepted November 26, 2013

ABSTRACT

Single-stranded (ss) DNA binding (SSB) proteins play central roles in DNA replication, recombination and repair in all organisms. We previously showed that *Escherichia coli* (*Eco*) SSB, a homotetrameric bacterial SSB, undergoes not only rapid ssDNA-binding mode transitions but also one-dimensional diffusion (or migration) while remaining bound to ssDNA. Whereas the majority of bacterial SSB family members function as homotetramers, dimeric SSB proteins were recently discovered in a distinct bacterial lineage of extremophiles, the *Thermus–Deinococcus* group. Here we show, using single-molecule fluorescence resonance energy transfer (FRET), that homodimeric bacterial SSB from *Thermus thermophilus* (*Tth*) is able to diffuse spontaneously along ssDNA over a wide range of salt concentrations (20–500 mM NaCl), and that *Tth*SSB diffusion can help transiently melt the DNA hairpin structures. Furthermore, we show that two *Tth*SSB molecules undergo transitions among different DNA-binding modes while remaining bound to ssDNA. Our results extend our previous observations on homotetrameric SSBs to homodimeric SSBs, indicating that the dynamic features may be shared among different types of SSB proteins. These dynamic features of SSBs may facilitate SSB redistribution and removal on/from ssDNA, and help recruit other SSB-interacting proteins onto ssDNA for subsequent DNA processing in DNA replication, recombination and repair.

INTRODUCTION

Single-stranded (ss) DNA binding (SSB) proteins are ubiquitous and found in bacterial, archaeal and eukaryotic cells, mitochondria, phages and viruses (1–4). SSB proteins bind specifically to ssDNA with high affinity in a sequence-independent manner, protect ssDNA from nucleolytic digestion and prevent intrastrand pairing (i.e. hairpin formation), in order to keep ssDNA in a suitable conformation for the action of enzymes involved in DNA replication, repair and recombination (5). In addition, SSB proteins control the accessibility of ssDNA and can physically interact with a variety of cellular genome maintenance proteins through the highly conserved C-terminal tails of SSB, including nucleases, helicases, polymerases, DNA damage signaling and strand-exchange proteins (3–5), to stimulate their activities. For example, *Escherichia coli* SSB is able to interact directly with at least 14 other proteins, including DNA Polymerase II, III and V, primase, RecQ, RecO, RecJ, RecG, PriA, PriB, Exonuclease I and IX, Uracil DNA Glycosylase and phage N4 RNA polymerase (5), bringing them to their sites of function.

SSB proteins are characterized by the presence of structurally conserved oligosaccharide/oligonucleotide binding (OB)-fold domains (6–8) for ssDNA binding. The majority of bacterial SSB proteins have a single OB fold per polypeptide and function as homotetramers. *Eco*SSB is the best studied example of homotetrameric SSB proteins and has served as the prototypical SSB protein for decades of study (1,9,10). Eukaryotic human mitochondrial SSB, like *Eco*SSB, also encodes a single OB fold per monomer and functions as stable homotetramers (11). In contrast, replication protein A (RPA), the major SSB proteins in eukaryotes, is a heterotrimeric protein complex composed of three distinct subunits and contains six OB folds per heterotrimer (2,12). Interestingly, SSB proteins from the *Thermus–Deinococcus* genera of bacteria were recently identified as stable homodimers in solution with two OB folds per monomer, contrast to the homotetrameric form so far found in bacteria. The two OB folds of homodimeric SSBs within each monomer have distinct amino acid

*To whom correspondence should be addressed. Email: tjha@illinois.edu

sequences and the functional SSB homodimer possesses only two highly conserved C-terminal tails whereas homotetrameric SSBs have four per tetramer (13–18).

Thermus thermophilus (*Tth*) SSB is a representative homodimeric SSB in the *Thermus–Deinococcus* group. The amino acid sequence of *Tth*SSB shares 43%, 44%, 44%, 44%, 43%, 48% and 82% identity with *Deinococcus radiodurans* (*Dra*), *Deinococcus radiopugnans*, *Deinococcus geothermalis*, *Deinococcus grandis*, *Deinococcus proteolyticus*, *Deinococcus murrayi* and *Thermus aquaticus* SSBs, respectively (15,16,19–21). Structural analysis of homodimeric SSBs indicated that although homodimeric SSBs share a similar tertiary arrangement within each OB fold as seen in homotetrameric SSBs, the quaternary arrangement of the four OB folds in the protein's active form is considerably different from that in homotetrameric SSBs (13,17,18). *Escherichia coli* maintains 200–3000 *Eco*SSB tetramers per cell and does not increase SSB levels significantly in response to DNA-damaging conditions, whereas in *Deinococcus radiodurans* the 20 000 *Dra*SSB dimers per cell increase to 56 000 dimers in response to ionizing radiation (13). The large number of *DraS*SB per cell and its rapid change in expression level in response to ionizing radiation are responsible for the high tolerance of *Dra* to the DNA-damaging condition (22). These results indicate that the homodimeric SSBs found in extremeophiles may have an expanded role in DNA metabolism. A recently resolved *Dra*SSB/ssDNA binding complex structure implied that although the ssDNA wraps around a *Dra*SSB homodimer in a similar way as seen in the *Eco*SSB/ssDNA complex, there are considerably more unstructured ssDNA regions in the *Dra*SSB-bound ssDNA, presumably due to an overall weaker protein–DNA interaction in the *Dra*SSB/ssDNA complex (23). Biochemical studies indicated that the binding affinities of homodimeric SSBs to ssDNA are considerably lower than that of *Eco*SSB under similar conditions ($K_d < 10^{-7}$ M for *Dra*SSB, in 1 M NaCl; $K_d < 10^{-9}$ M for *Eco*SSB, in 1 M NaBr); the affinity decreases as salt concentration increases, similar to *Eco*SSB (24,25).

Using *Eco*SSB as the prototypical SSB protein, we previously showed that *Eco*SSB can diffuse (or slide) on ssDNA spontaneously with an estimated diffusion coefficient of 300 (nucleotide)^2/s at 37°C, and that the diffusional migration of *Eco*SSB transiently melts DNA-hairpin structures and stimulates RecA filament elongation (26). We also showed that *Eco*SSB-interacting proteins can moderately slow *Eco*SSB diffusion on ssDNA by physically interacting with the last 8–10 amino acids within the conserved SSB C-terminal tail, raising the possibility that SSB acts as a mobile platform on ssDNA for the replication, repair and recombination machinery (27). However, it is not clear whether the diffusion activity observed for homotetrameric SSBs is general for other types of SSBs.

SSB binds ssDNA in different binding modes characterized by the length of ssDNA that it contacts and the number of ssDNA-binding domains involved (1,12,24,28). For *Eco*SSB, the relative stabilities of these binding modes largely depend on salt concentration and protein binding density: (i) at low monovalent salt concentrations (<20 mM NaCl) and high protein to DNA ratios, an *Eco*SSB tetramer occludes ~35 nt with high inter-tetramer cooperativity using only two out of four OB folds [termed the $(SSB)_{35}$ mode]. (ii) At high salt concentrations (≥200 mM NaCl), an *Eco*SSB tetramer occlude ~65 nt with low cooperativity using all four OB folds [termed the $(SSB)_{65}$ mode] (1,24). Furthermore, we previously observed direct transitions between the $(SSB)_{35}$ and $(SSB)_{65}$ binding modes in the presence of 10–100 nM *Eco*SSB and at low or intermediate salt concentrations (≤200 mM NaCl), and showed that 70-nt ssDNA with two *Eco*SSB tetramers bound can undergo dynamic structural rearrangement between two conformations [termed $(SSB)_{35}$ and $(SSB)_{35b}$ modes] (29). The occluded site size of a homodimeric SSB from the *Thermus–Deinococcus* group shows much more reduced dependence on salt concentration than that of an *Eco*SSB tetramer (15,19–21,24,30–32). For example, the occluded site size of a *Dra*SSB dimer is 45–47 nt at low salt concentrations (<20 mM NaCl) and increases to 50–55 nt at high salt concentrations (≥200 mM NaCl) (24,31,32). Therefore, it is unclear whether homodimeric SSBs can undergo similar binding mode transitions as seen in *Eco*SSB.

In this study, we use single molecule (sm) fluorescence resonance energy transfer (FRET) (33,34) to demonstrate that *Tth*SSB, a representative homodimeric SSB, is capable of rapid diffusion along ssDNA, implying that the diffusion activity may be shared among different types of SSB proteins. We also show that the small-scale (tens of nucleotides) *Tth*SSB diffusion along ssDNA is important in the fast redistribution of *Tth*SSB on ssDNA after its initial binding to a random ssDNA location, and that *Tth*SSB can transiently destabilize short DNA hairpins by diffusing in from ssDNA to an adjacent DNA hairpin. Furthermore, we present direct evidence that *Tth*SSB undergoes rapid binding mode transitions in the presence of free SSB proteins, extending our previous observations on homotetrameric *Eco*SSB to homodimeric SSBs.

MATERIALS AND METHODS

DNA sequences and annealing procedures

DNA oligonucleotides used for the sm experiments are listed below. '/iAmMC6T/' represents amine-modified thymine that is used to label the DNA with Cy3. Biotin modification was used for the surface immobilization.

(i) 5′-/Cy5/ GCC TCG CTG CCG TCG CCA-/biotin/-3′.
(ii) 5′-TGG CGA CGG CAG CGA GGC $(T)_{60}$ -/Cy3/-3′.
(iii) 5′-TGG CGA CGG CAG CGA GGC $(T)_{59}$ /iAmMC6T/ $(T)_n$ -3′, where n = 4, 8, 12 or 16.
(iv) 5′-TGG CGA CGG CAG CGA GGC-/Cy3/-$(T)_{58}$ -3′.
(v) 5′-/biotin/TGG CGA CGG CAG CGA GGC-/Cy5/-3'.
(vi) 5′-GGG CGG CGA CCT /iAmMC6T/ $(T)_{59}$ GCC TCG CTG CCG TCG CCA-3′.

(vii) 5′-AGG TCG CCG CCC-3′.
(viii) 5′-TGG CGA CGG CAG CGA GGC $(T)_{65}$ /iAmMC6T/ TGT GAC TGA GAC AGT CAC TT-/Cy5/-T-3′.

'/Cy3/' and '/Cy5/' represent the Cy3 and Cy5 fluorophores, respectively, which were attached directly to the DNA backbone using phosphoramidite chemistry. The partial duplex DNA substrates carrying Cy3 and Cy5 were annealed by mixing ~5 μM of biotinylated strand and ~7 μM of non-biotinylated strand in 10 mM Tris–HCl (pH 8.0) and 50 mM NaCl, followed by slow cooling from 90°C to room temperature for ~2 h.

Protein expression and purification

Thermus thermophilus (*Tth*) HB8 SSB proteins were expressed and purified as previously described (35,36). All protein concentrations cited in the text refer to *Tth*SSB dimers.

Sample assembly and data acquisition

smFRET experiments were performed at (23 ± 1)°C unless specified otherwise. Of partial duplex DNA substrates, 50–100 pM were immobilized on a quartz slide surface which is coated with polyethylene glycol (PEG) (mPEG-SC, Laysan Bio) in order to eliminate nonspecific surface adsorption of proteins (34). The immobilization was mediated by biotin–Neutravidin binding between biotinylated DNA, Neutravidin (Pierce) and biotinylated PEG (Bio-PEG-SC, Laysan Bio). For the experiments shown in Figures 1–5, 1nM *Tth*SSB were added into the sample chamber and incubated with the surface-tethered DNA substrates for 5 min in Buffer A containing 20 mM Tris–HCl (pH 8.0), 500 mM NaCl and 0.1 mg/ml BSA. A buffer wash step was then performed using Buffer A to flush out the excess unbound proteins. Finally, buffer B containing 20 mM Tris–HCl (pH 8.0), 0.1 mg/ml BSA, 2% (v/v) glycerol, 1 % (w/v) D-glucose, 165 U/ml glucose oxidase, 2170 U/ml catalase, 3 mM Trolox and indicated amount of NaCl were injected into the sample chamber before data acquisition. For the experiments shown in Figures 6 and 7, buffer B with desired *Tth*SSB concentration was directly injected into the sample chamber for data acquisition after immobilizing the DNA substrates. The single molecule data were acquired using total internal reflection fluorescence (TIRF) microscope (37) with a time resolution of ~30 ms. In some circumstances where the experiment needs to be performed at lower temperatures, a water-circulating bath circulator (NESLAB RTE-7 Digital One; Thermo Scientific) was used to cool down the sample stage, objective and prism-holder all together. The temperature of the outer surface of the sample chamber was measured by a handhold digital thermometer (Omega) as the best estimation of the experimental temperature inside the sample chamber.

FRET efficiency calculation

Apparent FRET efficiency was calculated from the fluorescence intensities of the donor (I_D) and acceptor (I_A) using the formula $E_{FRET} = I_A/(I_A + I_D)$. The background and the cross-talk between the donor and acceptor were corrected for as previously described (34). The smFRET histograms were built from >5000 surface-tethered DNA molecules.

Cross-correlation analysis

The cross-correlation analysis was performed as previously described (38,39). The cross-correlation curves were calculated between donor and acceptor fluorescence intensity-time traces obtained from each DNA molecule carrying a donor and an acceptor, and were then averaged over >100 DNA molecules. All cross-correlation curves presented are average curves. We determined the characteristic time, τ, by fitting the average cross-correlation curve to a single exponential function.

RESULTS

*Tth*SSB binding brings the two ends of bound ssDNA in close proximity

First, we employed smFRET, a single-molecule method to sensitively monitor the redistribution and changes of distance between a donor and an acceptor fluorophore in the range of 3–8 nm (34), to examine the binding of a single *Tth*SSB dimer to a short stretch of ssDNA. A partial duplex DNA substrate containing a 3′ 60-nt Poly(T) overhang [referred as $(dT)_{60}$] was immobilized on a surface passivated with PEG. A donor (Cy3) and an acceptor (Cy5) were attached near the two ends of the 60-nt ssDNA overhang, respectively, so that the FRET efficiency between them reports on the conformations of the 60-nt ssDNA (Figure 1A). The occluded site size of a *Tth*SSB dimer is expected to be ~45–55 nt with a slight dependence on salt concentration, similar to other homodimeric SSBs in the *Thermus–Deinococcus* group (24,30,31). The 60-nt ssDNA overhang can hence accommodate only one *Tth*SSB dimer in its fully wrapped binding mode. Indeed, previous studies using gel mobility shift assays have shown that $(dT)_{60}$ can efficiently accommodate only one *Tth*SSB dimer (14).

Before adding the proteins, a low FRET peak was observed for $(dT)_{60}$ in the smFRET histograms (Figure 1B) due to the large end-to-end distance of the 60-nt ssDNA region. As we increased salt concentration from 20 to 500 mM NaCl, the FRET peak position for $(dT)_{60}$ alone moved from ~0.05 to ~0.2 due to the increased ssDNA flexibility (or compaction) at higher salt concentrations (40). 1 nM *Tth*SSB dimers were then added into the sample chamber and incubated with the surface-tethered DNA substrates for 5 min at 500 mM NaCl, followed by a buffer wash to flush out excess unbound *Tth*SSB proteins. Upon *Tth*SSB binding, a much higher FRET peak centered at ~0.8 was observed at 500 mM NaCl even after the buffer wash (Figure 1B). Because *Tth*SSB remains bound to $(dT)_{60}$ for more than 2 h in the absence of unbound proteins (data not shown), we subsequently flowed in buffers containing different salt concentrations (but with no free SSB proteins) for data acquisition. The observed FRET peak values were ~0.74 and ~0.63 for 100 and 20 mM NaCl, respectively

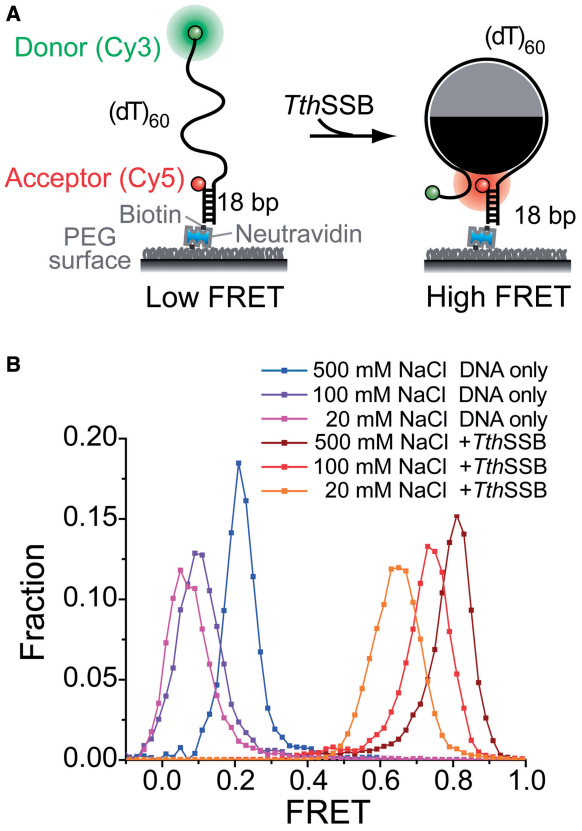

Figure 1. smFRET assays that report the conformations of *Tth*SSB-bound ssDNA. (**A**) A schematic illustration of our sm FRET experimental design for *Tth*SSB. A partial duplex DNA substrate [$(dT)_{60}$] was immobilized on a PEG-coated surface. Cy5 and Cy3 were attached to the ss–dsDNA junction and the end of the ssDNA overhang, respectively. (**B**) The smFRET histograms for $(dT)_{60}$ DNA alone and *Tth*SSB binding to $(dT)_{60}$ at different salt concentrations. *Tth*SSB proteins were loaded onto $(dT)_{60}$ under high salt condition (500 mM NaCl) and unbound proteins were removed before data acquisition (see also Materials and methods section).

(Figure 1B). The significantly increased FRET efficiencies observed upon *Tth*SSB binding in a broad range of salt concentrations (20–500 mM NaCl) indicate that the binding of a *Tth*SSB dimer brings the two ends of the ssDNA region into close proximity, similar as seen in homotetrameric SSBs (10,29,41), and it is in good agreement with the recently reported structure of the *Dra*SSB/ssDNA complex (23). The slight decrease in FRET at decreased salt concentrations may result from either a difference in the *Tth*SSB occluded site size (24,30,31), a difference in the flexibility of unbound ssDNA regions (40), or both.

*Tth*SSB is capable of diffusion along ssDNA

To test whether *Tth*SSB can diffuse along ssDNA, we used the single-molecule diffusion detection assay previously developed for *Eco*SSB (26,37). In this assay, we used a partial duplex DNA with a 5′ 72-nt ssDNA overhang which consists of a $(dT)_{60}$ region and a 12-nt extension of mixture sequence [referred as $(dT)_{60+12m}$]. Cy3 and Cy5 were attached near the two ends of the $(dT)_{60}$ region (Figure 2A). Before adding the proteins, a low FRET peak centered at ~0.15 was observed for $(dT)_{60+12m}$ in the smFRET histogram (Figure 2B). Upon *Tth*SSB binding to $(dT)_{60+12m}$, a broad FRET peak centered at ~0.43 was observed (Figure 2B) and FRET-time traces obtained from single *Tth*SSB–DNA complexes displayed fast FRET fluctuations beyond measurement noise (Figure 2A), similar to those previously observed for *Eco*SSB diffusion on $(dT)_{69+12m}$ (26). These FRET fluctuations were markedly suppressed and a steady FRET value (~0.7) was observed when the 12-nt mixture sequence in the 72-nt ssDNA overhang was hybridized to its complementary DNA strand (Figures 2A and 2B). To exclude binding and dissociation of additional *Tth*SSB molecules as the cause of fluctuations, excess unbound *Tth*SSB was removed by a buffer wash step as described above for $(dT)_{60}$. We also ruled out local melting of the duplex portion as a source of FRET fluctuations (Supplementary Figure S1). Therefore, the FRET fluctuations are likely caused by transient excursions of *Tth*SSB from the $(dT)_{60}$ region to the 12-nt extension, i.e. one-dimensional *Tth*SSB diffusion.

To further quantify the time scale of FRET fluctuations, we calculated the average cross-correlation of the donor and acceptor fluorescence intensities from >100 fluorescence intensity-time traces of single $(dT)_{60+12m}$ molecules in each condition (27,39). Anti-correlation between donor and acceptor intensities was only observed for *Tth*SSB-bound $(dT)_{60+12m}$ without hybridization of the 12-nt extension, and the single exponential fit to the average cross-correlation curve yielded a time scale of FRET fluctuations, $\tau = (61 \pm 11)$ ms (Figure 2C). Cross-correlation analysis showed no significant anti-correlation for either unbound $(dT)_{60+12m}$ or *Tth*SSB-bound hybridized $(dT)_{60+12m}$ (Figure 2C).

The time-averaged position of a diffusing *Tth*SSB is near the center of ssDNA

To further test *Tth*SSB diffusion on ssDNA, we designed a series of partial duplex DNA substrates containing 3′ Poly(T) overhangs of different lengths [referred as $(dT)_{60+n}$]. The ssDNA overhang is slightly longer than the occluded site size of a *Dra*SSB dimer, and consists of a $(dT)_{60}$ region with Cy3 and Cy5 attached near its ends (Figure 3A) and a $(dT)_n$ extension (n = 0, 4, 8, 12 or 16). When n = 0, $(dT)_{60+n}$ is the substrate we used in Figure 1. Before adding the protein, all of the $(dT)_{60+n}$ substrates showed a single low FRET peak centered at ~0.2 in the smFRET histograms at 500 mM NaCl (Figure 3B). After incubation with 1 nM *Tth*SSB dimer in 500 mM NaCl and the buffer wash step, a single peak centered at a higher FRET value was observed in the smFRET histograms for all five DNA substrates (Figure 3C). Interestingly, the average cross-correlation curves determined from >100 fluorescence intensity-time traces of single *Tth*SSB-bound $(dT)_{60+n}$ molecules showed no significant anti-correlation between Cy3 and Cy5 fluorescence intensities (Figure 3D), indicating that FRET fluctuations, which are expected from *Tth*SSB diffusion, could not be well detected with our experimental time resolution (~30 ms). Given that *Tth*SSB has high affinity to Poly(T) and would

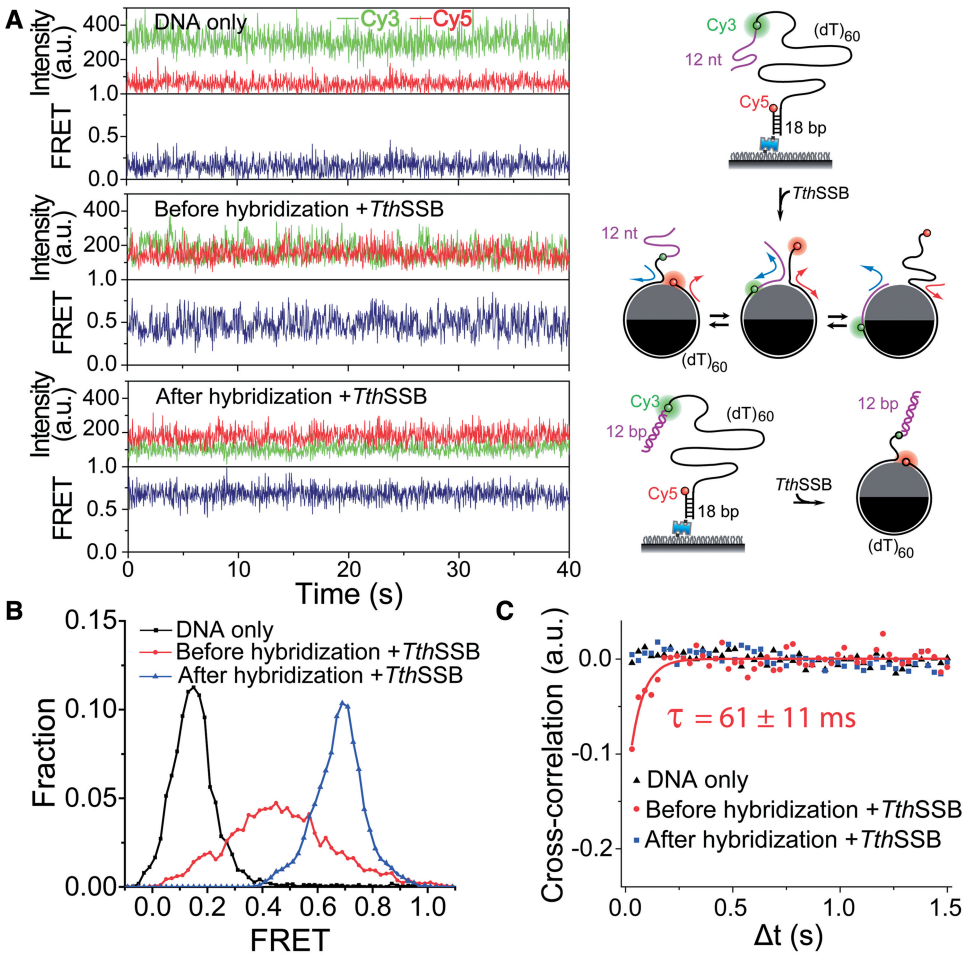

Figure 2. Protein diffusion detection assays based on DNA hybridization. (**A**–**C**) Representative single-molecule time traces (A), smFRET histograms (B) and average cross-correlation curves (C), for $(dT)_{60+12m}$ DNA alone and *Tth*SSB-bound $(dT)_{60+12m}$ with and without the hybridization to the 12-nt mixture sequence ssDNA region. FRET fluctuations beyond measurement noise were detected only when the 12-nt extension is available for *Tth*SSB binding. Unbound proteins were removed before data acquisition such that the FRET flucatuations reflect only the repositioning of the bound *Tth*SSB along $(dT)_{60+12m}$. For simplification, the 18-bp duplex DNA region is not shown for *Tth*SSB-bound $(dT)_{60+12m}$ in (A). The solid line in (C) is a fit to a single exponential function.

generally not slide off the ssDNA tail, we considered two possible explanations for this observation: (i) after its initial binding to a random position along the ssDNA overhang, *Tth*SSB is unable to move along $(dT)_{60+n}$, resulting in a time-independent single FRET state for each *Tth*SSB-bound $(dT)_{60+n}$ molecule. (ii) After its initial binding to a random position along ssDNA, *Tth*SSB is able to move along $(dT)_{60+n}$, but the movement is too fast to be detected within our 30-ms time resolution, resulting in a time-averaged FRET value for each *Tth*SSB-bound $(dT)_{60+n}$ molecule. For the first explanation, one would expect that the sm FRET-efficiency distribution of $(dT)_{60+n}$ with a larger n value should be broader with *Tth*SSB bound and should include all the FRET efficiency values observed for *Tth*SSB-bound $(dT)_{60+m}$ (here $m < n$), because a longer overhang should provide more possible binding positions (i.e. more diverse FRET efficiency values) for *Tth*SSB. However, the single peak of the smFRET histogram, instead of becoming broader, is shifted towards a lower FRET value as n increases (Figure 3C), disfavoring the first explanation. Therefore, we favor the second explanation in which *Tth*SSB rapidly diffuses along the entire length of the ssDNA overhang and appears to be positioned near the center of the overhang within our 30-ms time resolution. This time-averaging effect has also been observed in other smFRET studies (42,43).

All of the measurements above for $(dT)_{60+n}$ were conducted at room temperature (23°C) and in 500 mM NaCl. As a further test for the second explanation, we repeated the experiments at room temperature (23°C) and lower temperatures (18, 14 and 11°C) and in 100 mM NaCl for $(dT)_{60+4}$ (Figure 4). Previously, we demonstrated that lowering the temperature slows *Eco*SSB diffusion on ssDNA (26). Indeed, we were able to observe FRET fluctuations beyond measurement noise in the FRET-time traces of *Tth*SSB-bound $(dT)_{60+4}$ at 18, 14 and 11°C (Figure 4A). We excluded the possibility of local wrapping–unwrapping of ssDNA on *Tth*SSB by conducting the experiment at the same condition (100 mM NaCl, 11°C) on the $(dT)_{60}$ substrate with Cy3 and Cy5 attached near the two ends of the ssDNA overhang (Supplementary

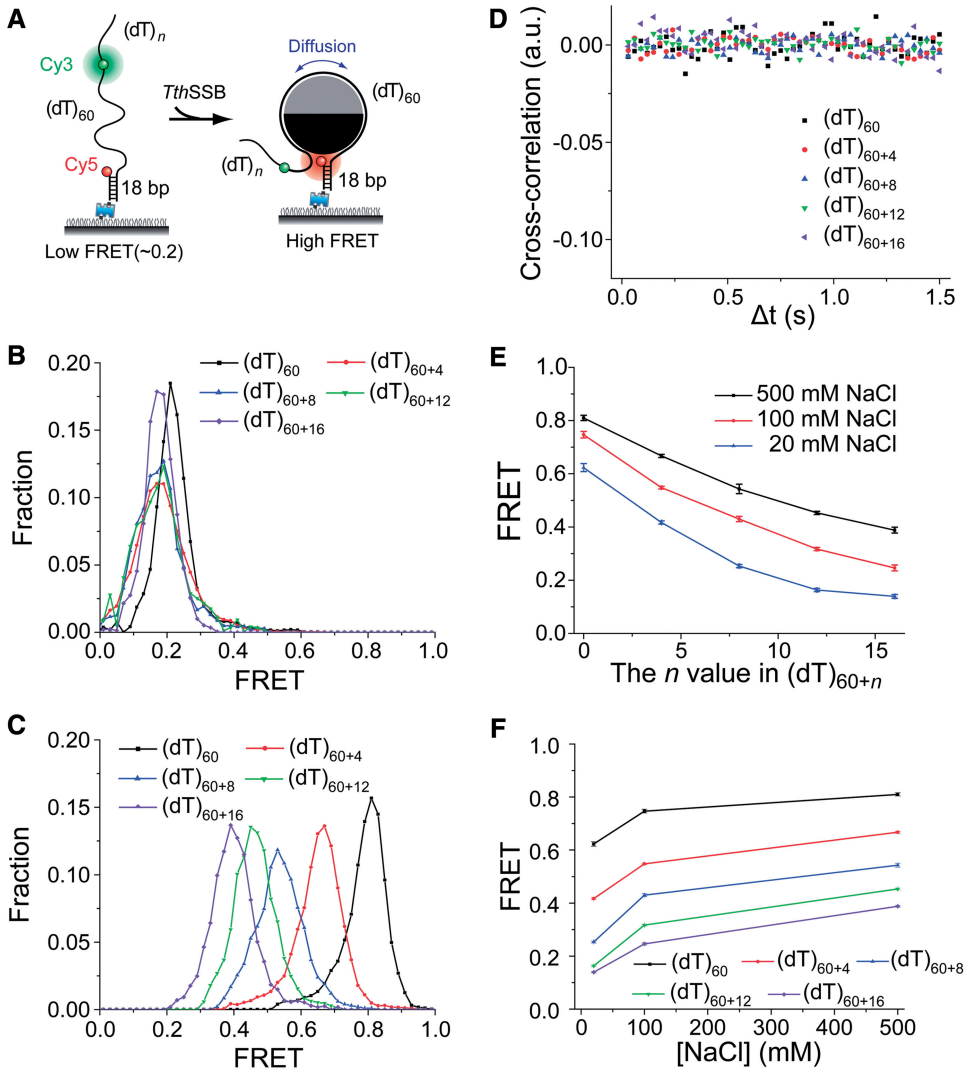

Figure 3. *Tth*SSB appears to be positioned near the center of the $(dT)_{60+n}$ ssDNA overhangs though rapid diffusion. (**A**) A schematic illustration of our experimental design for $(dT)_{60+n}$ (n = 0, 4, 8, 12 or 16). Cy3 and Cy5 were attached to the ss–dsDNA junction and the middle of the ssDNA overhang, respectively, separated by $(dT)_{60}$. (**B**) The smFRET histograms of $(dT)_{60+n}$ DNA in the absence of proteins, obtained at 500 mM NaCl. (**C**) smFRET histograms for *Tth*SSB-bound $(dT)_{60+n}$, obtained at 500 mM NaCl, showing a single narrow FRET peak. (**D**) Average cross-correlation curves for *Tth*SSB-bound $(dT)_{60+n}$, obtained at 500 mM NaCl, indicating no significant FRET fluctuations. (**E**) The FRET value at the FRET peak position versus the n value in $(dT)_{60+n}$, obtained at 20, 100 or 500 mM NaCl. (**F**) The FRET value at the FRET peak position versus the salt concentration for different $(dT)_{60+n}$ substrates. *Tth*SSB proteins were loaded onto $(dT)_{60}$ under high salt condition (500 mM NaCl) and unbound proteins were removed before the buffer containing a lower NaCl concentration was added to the sample chamber.

Figure S3). FRET fluctuations were due to anti-correlated fluctuations of the donor and acceptor intensities, as confirmed by the cross-correlation analysis (Figure 4C), which yielded the fluctuation time scales: $\tau(23°C) = (67 \pm 28)$ ms, $\tau(18°C) = (79 \pm 31)$ ms, $\tau(14°C) = (83 \pm 20)$ ms, and $\tau(11°C) = (88 \pm 13)$ ms. The Arrhenius fit of $\ln(1/\tau)$ versus $1/T$ (Figure 4D) gave an apparent activation energy of $E_a = (16 \pm 3)$ kJ/mol for *Tth*SSB diffusion, which is smaller than the E_a determined for *Eco*SSB diffusion on ssDNA [~(81 ± 7) kJ/mol] (26).

Having demonstrated that *Tth*SSB is capable of diffusion on $(dT)_{60+n}$ under high and intermediate salt condition (500 and 100 mM NaCl), we next tested *Tth*SSB diffusion at low salt concentrations. After loading a *Tth*SSB dimer onto surface-tethered $(dT)_{60+n}$ in 500 mM NaCl, we flushed out unbound proteins with a buffer also containing 500 mM NaCl. A buffer containing either 100 or 20 mM NaCl was subsequently flowed into the sample chamber before data acquisition. At both 20 and 100 mM NaCl, we observed similar results as at 500 mM NaCl: a single narrow peak was observed in the smFRET histogram (data not shown) and is shifted towards a lower FRET value as n increases (Figure 3E), suggesting that *Tth*SSB diffuses on $(dT)_{60+n}$ in a wide range of salt concentrations (20–500 mM NaCl). As discussed above for $(dT)_{60}$, the slight decrease in FRET efficiency at decreased salt concentrations for each $(dT)_{60+n}$ substrate (Figure 3F) may result from either a difference in the *Tth*SSB occluded site size (24,30,31), a difference in the flexibility of unbound ssDNA regions (40), or both.

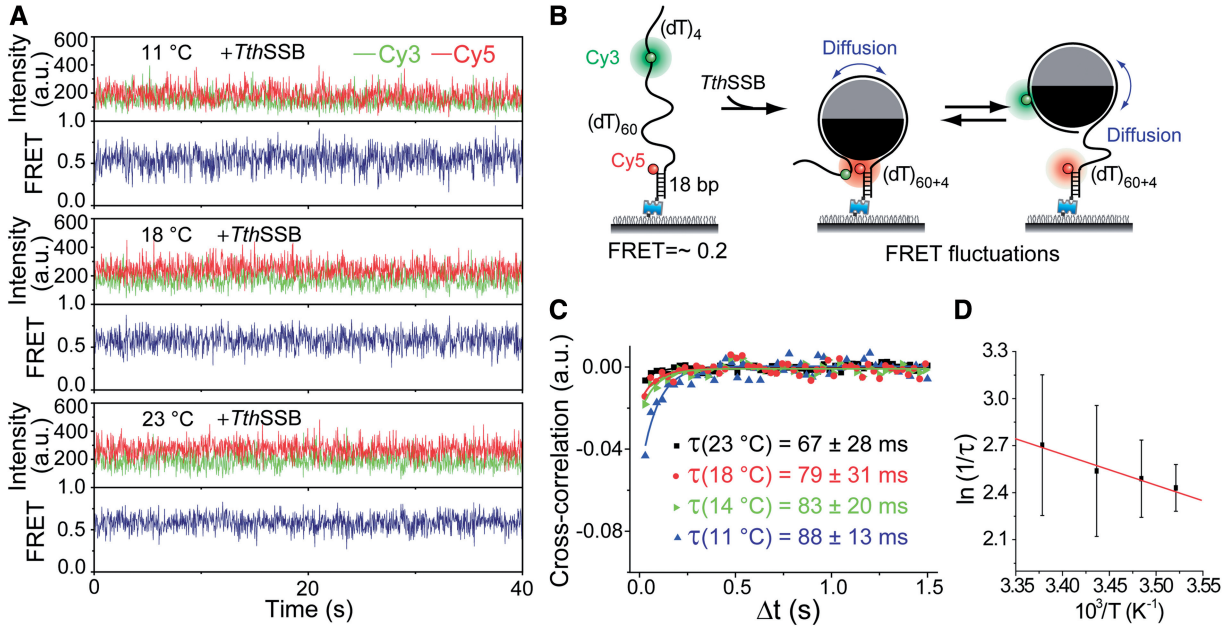

Figure 4. Lower temperatures slow *Tth*SSB diffusion on $(dT)_{60+4}$. (**A**) Representative single-molecule time traces for *Tth*SSB-bound $(dT)_{60+4}$ obtained at different temperatures (23, 18, 14 and 11°C) and at 100 mM NaCl. (**B**) A schematic illustration of our experimental design, showing how *Tth*SSB diffusion may result in FRET fluctuations. (**C**) Average cross-correlation curves for *Tth*SSB-bound $(dT)_{60+4}$ obtained at different temperatures and at 100 mM NaCl. More significant FRET fluctuations beyond measurement noise were detected at lower temperatures. The time scales of the FRET fluctuations were determined from fits to a single exponential function (solid lines). Unbound proteins were removed before data acquisition. (**D**) Arrhenius plot of apparent rates as a function of 1/T.

*Tth*SSB diffusion transiently destabilizes short DNA-hairpin structures

The single molecule studies have shown homotetrameric SSBs are able to transiently disrupt short DNA-hairpin structures (26,44). To further demonstrate the functional role of *Tth*SSB diffusion, we examined whether *Tth*SSB can use its diffusion activity to transiently destabilize DNA-hairpin structures. We designed a partial duplex DNA containing a 3′ $(dT)_{65}$ ssDNA overhang with a 7-bp internal hairpin located at the 3′-end of the overhang [referred as $(dT)_{65+hp+3}$]. Cy3 and Cy5 were attached to the ends of the hairpin sequence such that FRET reports the formation or melting of the hairpin (Figure 5A). Before adding the proteins, $(dT)_{65+hp+3}$ exhibited steady high FRET (~0.9) in the smFRET-time traces obtained at 500 mM NaCl, suggesting that the hairpin itself is stably formed at room temperature (Figure 5A). After incubation with 1 nM *Tth*SSB dimer in 500 mM NaCl and the buffer wash step, a number of brief excursions to a low FRET state (~0.5) were observed in FRET-time traces, indicating transient unzipping and reformation of the hairpin. Cross-correlation analysis yielded the time scale of FRET fluctuations $\tau = (420 \pm 36)$ ms (Figure 5B). As the $(dT)_{65}$ region is slightly larger than the occluded site size of a *Tth*SSB dimer, one *Tth*SSB dimer is expected to remain bound to the $(dT)_{65}$ region after the buffer wash. Since the unbound proteins were flushed out before the data acquisition, the transient melting of the hairpin must be due to the destabilization of the hairpin segment by *Tth*SSB.

Direct observation of binding mode transition and cooperative binding of *Tth*SSB

Previous ensemble studies have suggested that homodimeric SSBs, like homotetrameric SSBs, may undergo a transition between different binding modes, although the occluded site size of a homodimeric SSB showed a much more reduced salt concentration dependence than that of a homotetrameric SSB (24,30). Using smFRET, we previously showed that a partial duplex DNA substrate containing a $(dT)_{70}$ overhang may accommodate either one *Eco*SSB tetramer in the $(SSB)_{65}$ mode or two *Eco*SSB tetramers in the $(SSB)_{35}$ mode, and that a $(dT)_{70}$ molecule undergoes transitions between these two scenarios in the presence of *Eco*SSB proteins in solution (29). Given that *Tth*SSB dimers have a less salt-dependent occluded site size change (45–55 nt) compared to *Eco*SSB, we asked whether similar results can be obtained for *Tth*SSB on $(dT)_{60}$. Instead of flushing out the unbound proteins, we kept 1, 3, 6 or 10 nM *Tth*SSB dimers in solution and acquired the data at 20, 100 or 500 mM NaCl accordingly. Figure 6A shows representative FRET-time traces obtained from single *Tth*SSB-bound $(dT)_{60}$ molecules. Clear fluctuations between two discrete FRET states (referred as the high/low FRET state) were observed at 20 and 100 mM NaCl, but not at 500 mM NaCl. We determined the average transition rates between the two FRET states (Figure 6B).

Our observations agree with previous biophysical studies indicating that homodimeric SSBs show an enhanced intermolecular binding cooperativity at lower salt concentrations (23,30,31). Additionally, previous

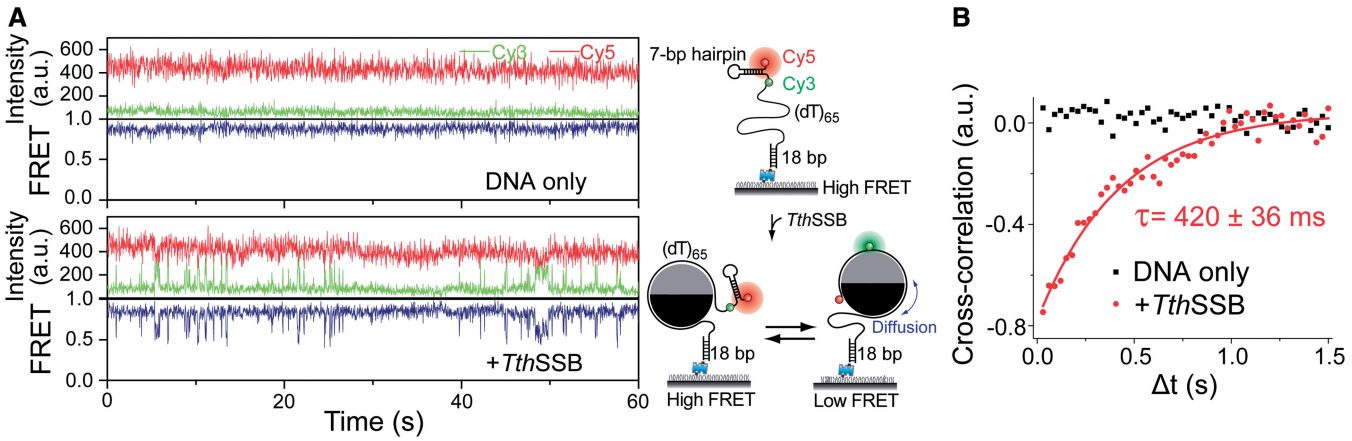

Figure 5. *Tth*SSB diffusion can transiently destabilize short DNA hairpin structures. (**A** and **B**) Representative single-molecule time traces (A) and average cross-correlation curves (B), for $(dT)_{65+hp+3}$ alone and *Tth*SSB-bound $(dT)_{65+hp+3}$, obtained at 500 mM NaCl. Unbound proteins were removed before data acquisition. The solid line in (B) is a fit to a single exponential function.

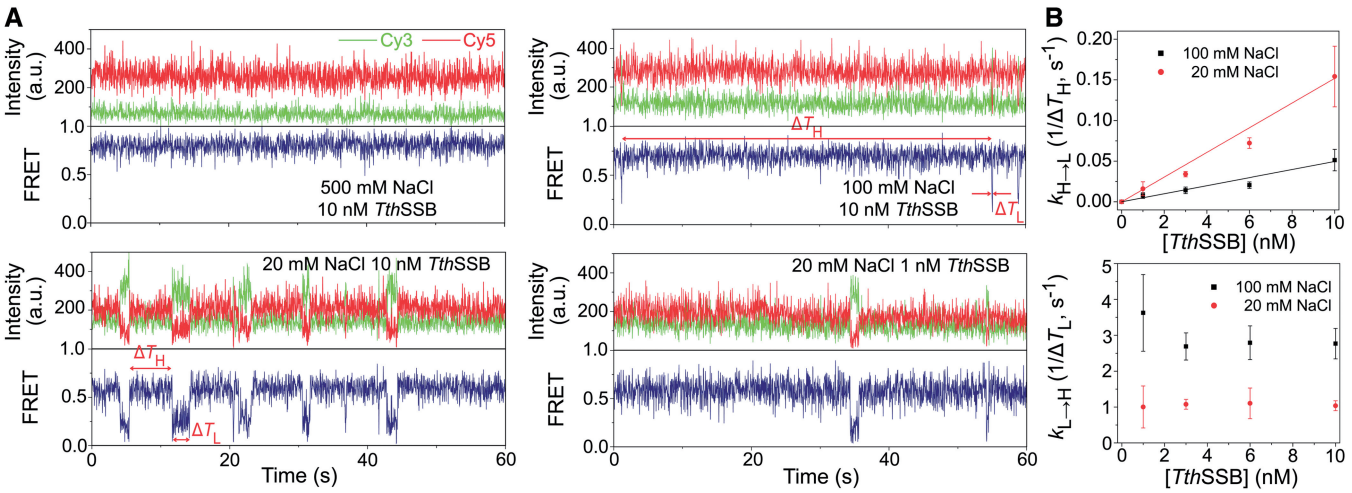

Figure 6. Transitions between different binding modes for *Tth*SSB binding to $(dT)_{60}$ in the presence of proteins in solution. (**A**) Representative sm FRET-time traces for *Tth*SSB-bound $(dT)_{60}$, obtained at 500 and 100 mM NaCl when 10 nM *Tth*SSB were present, and those obtained at 20 mM NaCl when 10 or 1 nM *Tth*SSB were present in the sample camber. 1 nM *Tth*SSB were first incubated with the surface-tethered $(dT)_{60}$ in 500 mM NaCl, followed by a buffer wash to remove unbound *Tth*SSB proteins. The buffer containing the indicated *Tth*SSB and NaCl concentration was then injected into the chamber for data acquisition. ΔT_H and ΔT_L represent the durations for the high and low FRET state, respectively. (**B**) Transtion rates of the interconversions between high and low FRET state ($1/\Delta T_H$ and $1/\Delta T_L$ represent the high to low FRET-state transiton and the low to high FRET-state transition, respectively), as a function of the *Tth*SSB concentration. Solid lines are the linear fits for high to low FRET-state transition rate as a function of *Tth*SSB concentration.

biochemical studies have shown that a homodimeric SSB binds up to two ssDNA molecules of $(dT)_{25}$ with a salt-dependent negative cooperativity: at either 20 and 200 mM NaCl, the second molecule of $(dT)_{25}$ has a weaker affinity to *Dra*SSB than the first $(dT)_{25}$ molecule, but such negative cooperativity (i.e. the difference in the affinities of the first and the second bound $(dT)_{25}$) is much larger at 20 mM NaCl than at 200 mM NaCl (24). The salt-dependent negative cooperativity observed for homodimeric SSBs predicts that the decrease in salt concentration would favor the transition from single bound protein to two bound proteins per $(dT)_{60}$ because larger negative cooperativity would favor a single *Tth*SSB dimer binding to about half of $(dT)_{60}$. Indeed, the transition rate from high FRET to low FRET states ($k_{H\rightarrow L}$) is larger at higher *Tth*SSB concentrations and at lower salt concentrations, whereas the transition rate from low to high FRET states ($k_{L\rightarrow H}$) does not depend on *Tth*SSB concentration but is smaller at lower salt concentrations (Figure 6B). We hence assigned the high FRET state to $(dT)_{60}$ with one *Tth*SSB dimer bound and the low FRET state to $(dT)_{60}$ with two *Tth*SSB dimers bound. In the low FRET state, two *Tth*SSB dimers bind to the same $(dT)_{60}$ molecule, with each *Tth*SSB dimer occupying 30-nt ssDNA region on average.

Next, we tested another DNA substrate with a longer ssDNA overhang $(dT)_{60+16}$ in the presence of 0.5–4 nM *Tth*SSB dimers in solution. Two-state transitions were also observed in the single molecule FRET-time traces at 20 and 100 mM NaCl, but not at 500 mM NaCl

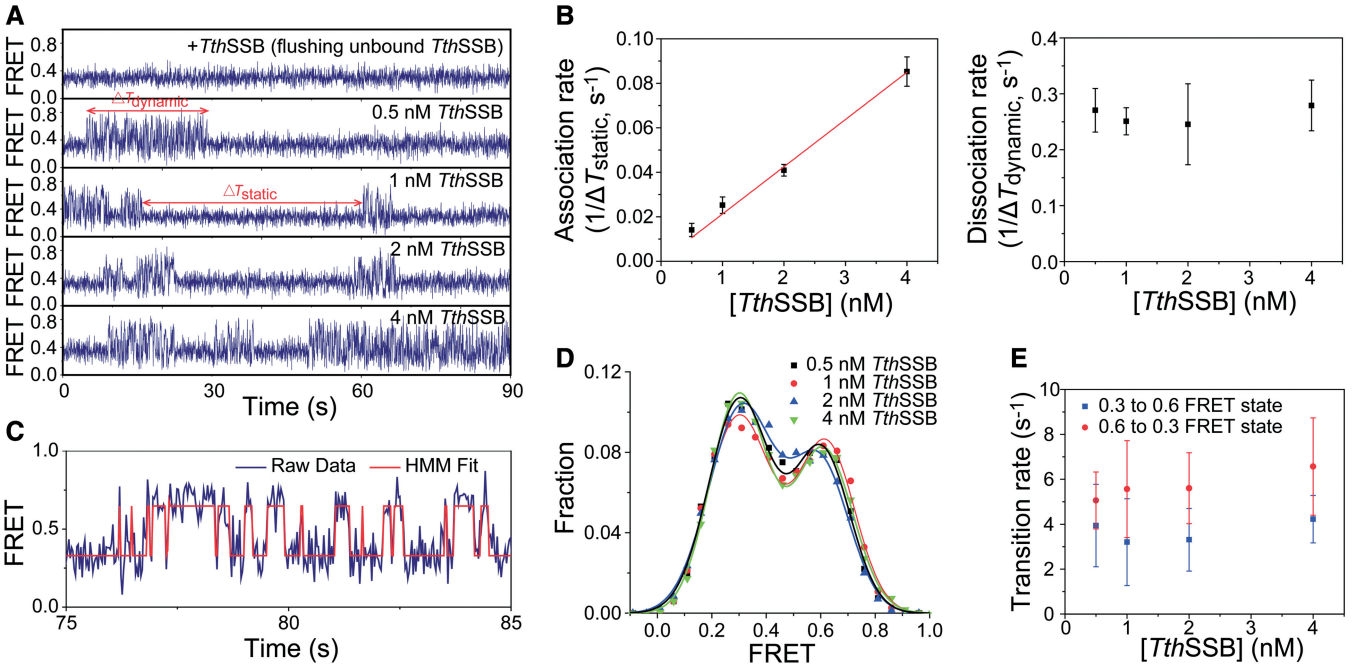

Figure 7. Transitions between different binding modes for *Tth*SSB binding to $(dT)_{60+16}$ in the presence of proteins in solution. (**A**) Representative sm FRET-time traces for *Tth*SSB-bound $(dT)_{60+16}$, obtained at 100 mM NaCl and when 0, 0.5, 1, 2 or 4 nM *Tth*SSB were present in the sample camber. $\Delta T_{dynamic}$ and ΔT_{static} represent the durations for the 'dynamic' and 'static' states, respectively. (**B**) Association and dissociation rates of the second *Tth*SSB to/from $(dT)_{60+16}$ ($1/\Delta T_{static}$ and $1/\Delta T_{dynamic}$, respectively), as a function of the *Tth*SSB concentration. (**C**) Hidden Markov model (HMM)-derived idealized FRET trajectory (red) superimposed on the FRET-time trace (blue), for a selected time period during which the molecule is in the 'dynamic' state. Two FRET states were determined from the HMM fit (~0.3 and ~0.6 FRET). (**D**) FRET-efficiency distributions within the 'dynamic' state at different *Tth*SSB concentrations (averaged from >50 molecules). Solid lines are the fits to a double-Gaussian function. (E) Transition rates between the 0.3 and 0.6 FRET state, determined from the HMM fit at different *Tth*SSB concentrations.

(Figures 7A and Supplementary Figure S2). One of the two states in the FRET-time traces displayed fast FRET fluctuations (referred as 'dynamic' state), whereas the other state displayed a steady FRET value (referred as 'static' state). We determined the average transition rates between the 'dynamic' and 'static' states, $1/\Delta T_{dynamic}$ and $1/\Delta T_{static}$ ($\Delta T_{dynamic}$ and ΔT_{static} represent average durations in the 'dynamic' and 'static' states, respectively). We found $1/\Delta T_{static}$, similar to $k_{H\rightarrow L}$, displays a linear dependence on *Tth*SSB concentration, whereas $1/\Delta T_{dynamic}$, similar to $k_{L\rightarrow H}$, is independent of *Tth*SSB concentration (Figure 7B). Therefore, we assigned the 'static' state to $(dT)_{60+16}$ with one *Tth*SSB dimer bound and the 'dynamic' state to $(dT)_{60+16}$ with two *Tth*SSB dimers bound. $1/\Delta T_{static}$ and $1/\Delta T_{dynamic}$ hence gave an association rate constant of $(2.1 \pm 0.1) \times 10^7 M^{-1} \cdot S^{-1}$ and a dissociation rate constant of $(0.26 \pm 0.07)\ S^{-1}$] for the second *Tth*SSB dimer binding and dissociation, respectively. Furthermore, we quantified the FRET fluctuations within the 'dynamic' state using an HMM-based statistical approach that determines the most likely time sequence of FRET states (Figure 7C) (45). FRET efficiency distributions within the 'dynamic' state can be fit well to a double-Gaussian function (Figure 7D), indicating the existence of two distinct FRET substates (referred as 0.3 and 0.6 FRET states, respectively). The transition rate from the 0.3 FRET to 0.6 FRET state was determined to be $(3.7 \pm 1.6)\ s^{-1}$, and the transition rate from 0.6 FRET to 0.3 FRET state was determined to be $(5.7 \pm 1.8)\ s^{-1}$, both of which are independent of *Tth*SSB concentration (Figure 7E). We therefore assigned the two FRET substates to two distinct structural arrangements of $(dT)_{60+16}$ with two *Tth*SSB dimers bound. The association of the second *Tth*SSB dimers results in a fast 'dynamic' FRET state for $(dT)_{60+16}$ but not for $(dT)_{60}$, probably because the dynamic structural rearrangement from the DNA molecule with two *Tth*SSB dimers bound requires the $(dT)_{16}$ extension.

DISCUSSION

In this study, we employed smFRET to study the dynamics of *Tth*SSB, a representative homodimeric SSB, binding to short ssDNA molecules ranging from 60 to 76 nt. Although their quaternary arrangements of the OB folds are different (13,17,18), both homotetrameric and homodimeric SSBs bind ssDNA in a way that brings the two ends of bound DNA in close proximity under high salt conditions, consistent with the recently resolved crystal structure of *Dra*SSB–ssDNA complex (23). Both types of SSBs are capable of rapid diffusion along ssDNA. Previously, we showed that even when the SSB–ssDNA structure is not fully wrapped and a small force (1–5 pN) is used to unwrap some ssDNA from the protein surface, *Eco*SSB diffusion on ssDNA still persists (27). Our results imply that the diffusion activity may be a shared property for different types of ssDNA-binding proteins. Besides SSB proteins, some

other proteins have also been reported to show similar one-dimensional random walk along ssDNA, including POT1-TTP diffusion on telomeric DNA (46) and RAD52 diffusion during homology search (47,48).

Similar to homotetrameric SSBs, *Tth*SSB can diffuse continually as long as there is an available extension of ssDNA beyond its occluded site size. The activation energy for *Tth*SSB diffusion is ~(16 ± 3) kJ/mol, smaller than that of *Eco*SSB diffusion [~(81 ± 7) kJ/mol] under a similar condition (26). The reduced activation energy of *Tth*SSB diffusion might result from the different residues of *Tth*SSB that interact with ssDNA compared to those of *Eco*SSB, given that the amino acid sequence of the two OB folds in each *Tth*SSB monomer (i.e. the N- and C-terminal OB folds) only share 32% and 40% identity, respectively, with *Eco*SSB's OB fold (14,15). SSB OB folds bind to ssDNA through a combination of base-stacking, electrostatic and polar interactions between protein residues and ssDNA, all of which are dependent on the amino acid sequence in the OB fold (23). For example, researchers have identified in *Eco*SSB four residues (W40, W54, F60, W88) engaged in the base-stacking interaction between its OB folds and ssDNA (13–15); in *Tth*SSB, the corresponding residues are L, Y, L, W for N-teminal OB fold and F, W, W for C-terminal OB fold (the residue corresponding to W40 could not be identified via sequence alignment), respectively (14,15). The different amino acid sequence present in *Thermus–Deinococcus* SSBs should be accounted for the lower DNA-binding affinity as well as the reduced activation energy for SSB diffusion on ssDNA. Besides, in the resolved crystal structure of the *Dra*SSB–ssDNA complex, the electron density of a considerable portion of the ssDNA that wraps around SSB protein was lost, indicating a relatively dynamic characteristics of the ssDNA at these positions, consistent with the low activation energy for the diffusion (23). Additionally, *Tth*SSB diffusion appears to be faster than that of *Eco*SSB, and is too fast to be detected for some DNA substrates [e.g. $(dT)_{60+n}$] with the 30-ms time resolution. This is consistent with the previous observation that the binding affinity of ssDNA for homodimeric SSBs is weaker than for *Eco*SSB (24) because SSB diffusion requires breakage and reformation of SSB–DNA interactions (27).

SSB diffusion may have multiple functional roles. First, rapid SSB diffusion along DNA should be important in redistributing SSB on ssDNA after its initial binding to a random DNA location, because for proteins with such high affinities, redistribution would be difficult if it required complete dissociation and reassociation. Second, SSB diffusion can transiently destabilize short DNA hairpin structures, probably due to trapping of spontaneously opened ends of the duplex region. We have shown that the hairpin removal by *Eco*SSB diffusion is responsible for the facilitated RecA filament growth (26). For *Tth*SSB, it has been shown that *Tth*SSB enhances the synthesis rate of DNA polymerases from *Tth* and *Pyrococcus* (49), and many different types of SSBs have been used to increase the amplification efficiency for the polymerase chain reaction (PCR) (50). Because specific interactions between polymerases and SSBs are not required for the stimulated activity, the observation is presumably due to SSB diffusion that removes DNA-hairpin structures. Third, SSB diffusion may provide a mechanism for how SSBs recruit other SSB-interacting enzymes onto ssDNA for subsequent DNA processing. We previously showed that specific interactions between *Eco*SSB and *Eco*RecO did not abolish but moderately slowed *Eco*SSB diffusion on ssDNA (27).

Furthermore, we presented direct evidence that *Tth*SSB undergoes rapid binding mode transitions in the presence of free SSB proteins in solution. Although the occluded site size of a homodimeric SSB displays less dependence on the salt concentration than that of an *Eco*SSB tetramer and ranges from 45 to 55 nt with increase in salt concentration (15,19–21,24,30–32), we observed transitions between a single bound protein and two bound proteins per ssDNA on $(dT)_{60}$ and $(dT)_{60+16}$ at low and intermediate salt concentrations (20–100 mM NaCl). When two *Tth*SSB dimers bind to the same 60- or 76-nt ssDNA molecule, the second *Tth*SSB has a weaker affinity to DNA than the first bound *Tth*SSB (i.e. negatively cooperative binding). Additionally, 76-nt ssDNA with two *Tth*SSB dimers bound may undergo dynamic structural rearrangement between two conformations. Similar observations were made previously for *Eco*SSB binding to $(dT)_{70}$ (29).

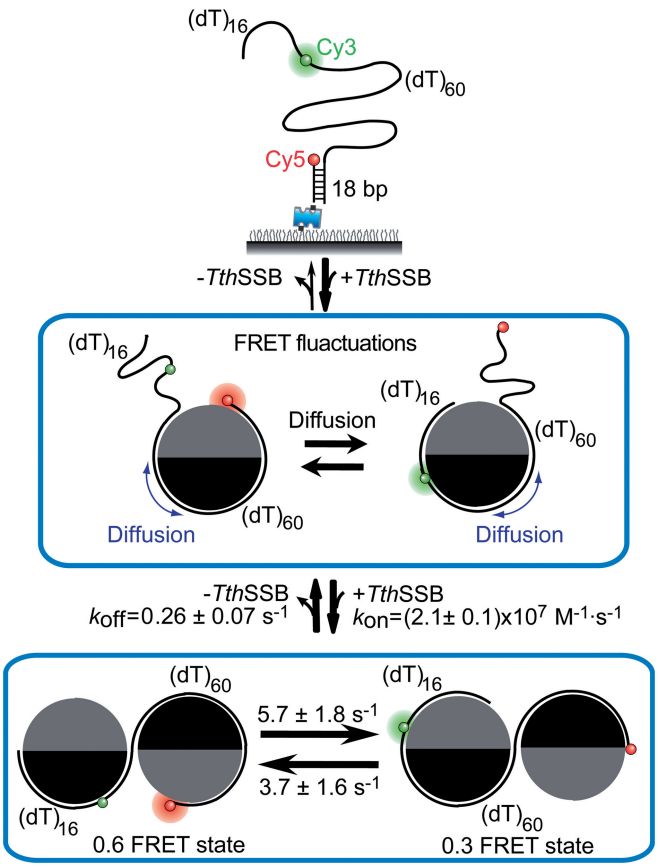

Figure 8. Model of *Tth*SSB dynamics on ssDNA. $(dT)_{60+16}$ is illustrated as the ssDNA template for *Tth*SSB binding. For simplification, only the ssDNA region is shown in the cartoon for *Tth*SSB-bound $(dT)_{60+16}$.

SSB-binding mode transition, depending on the local ionic strength and SSB concentrations, might play a role in controlling the accessibility of ssDNA in various biological processes by tuning the binding site size per SSB and intermolecular cooperativity of SSB proteins, exposing or shielding ssDNA region for other proteins to bind. In addition, SSB-binding mode transition can be regulated by SSB–protein interactions via highly conserved SSB C-terminal tails. Previous studies showed that PriC, a key protein for *E. coli* DNA replication restart, alters the structure of SSB/ssDNA binding complex and shifts the binding equilibrium towards the highly cooperative $(SSB)_{35}$ mode over the less cooperative $(SSB)_{65}$ mode, by interacting with *Eco*SSB's C-termial tails (51).

In summary, the data presented in this study extend our previous observations on homotetrameric *Eco*SSBs to homodimeric SSBs, and suggest that *Tth*SSB/DNA complexes are highly dynamic (Figure 8). Importantly, the covalent linkage between multiple non-identical OB-fold domains in *Tth*SSB dimers, which is also the signature of eukaryotic RPAs, does not preclude SSB diffusion or binding mode transitions. When only one *Tth*SSB dimer binds to an ssDNA region that is slightly longer than its occluded site size, it diffuses rapidly while remaining stably bound, which should be useful to cover and protect even small ssDNA gaps between two bound *Tth*SSBs and remove DNA hairpin structures. Additionally, *Tth*SSB/DNA complexes undergo dynamic interconversions among different binding modes and/or structural rearrangements if there are unbound proteins nearby. These dynamic features of SSB–DNA complex should be important for the functional roles of SSBs in genome maintenance and are possibly shared among different types of SSBs.

SUPPLEMENTARY DATA

Supplementary Data are available at NAR Online.

ACKNOWLEDGEMENTS

The authors thank all the members of Ha laboratory for experimental help and discussions.

FUNDING

National Institutes of Health [RR025341 and GM065367 to T.H.]; National Science Foundation [0822613 and 0646550 to T.H.]; JSPS KAKENHI Grant [22570147]; Howard Hughes Medical Institute (to T.H.). Funding for open access charge: NIH [RR025341 and GM065367 to T.H.]; National Science Foundation [0822613 and 0646550 to T.H.]; JSPS KAKENHI [22570147].

Conflict of interest statement. None declared.

REFERENCES

1. Lohman,T.M. and Ferrari,M.E. (1994) Escherichia coli single-stranded DNA-binding protein: multiple DNA-binding modes and cooperativities. *Annu. Rev. Biochem.*, **63**, 527–570.
2. Wold,M.S. (1997) Replication protein A: a heterotrimeric, single-stranded DNA-binding protein required for eukaryotic DNA metabolism. *Annu. Rev. Biochem.*, **66**, 61–92.
3. Nam,E.A. and Cortez,D. (2009) SOSS1/2: Sensors of Single-Stranded DNA at a Break. *Mol. Cell*, **35**, 258–259.
4. Richard,D.J., Bolderson,E. and Khanna,K.K. (2009) Multiple human single-stranded DNA binding proteins function in genome maintenance: structural, biochemical and functional analysis. *Crit. Rev. Biochem. Mol. Biol.*, **44**, 98–116.
5. Shereda,R.D., Kozlov,A.G., Lohman,T.M., Cox,M.M. and Keck,J.L. (2008) SSB as an Organizer/Mobilizer of Genome Maintenance Complexes. *Crit. Rev. Biochem. Mol.*, **43**, 289–318.
6. Theobald,D.L., Mitton-Fry,R.M. and Wuttke,D.S. (2003) Nucleic acid recognition by OB-fold proteins. *Annu. Rev. Biophys. Biomol. Struct.*, **32**, 115–133.
7. Murzin,A.G. (1993) OB(oligonucleotide/oligosaccharide binding)-fold: common structural and functional solution for non-homologous sequences. *EMBO J.*, **12**, 861–867.
8. Flynn,R.L. and Zou,L. (2010) Oligonucleotide/oligosaccharide-binding fold proteins: a growing family of genome guardians. *Crit. Rev. Biochem. Mol. Biol.*, **45**, 266–275.
9. Raghunathan,S., Ricard,C.S., Lohman,T.M. and Waksman,G. (1997) Crystal structure of the homo-tetrameric DNA binding domain of Escherichia coli single-stranded DNA-binding protein determined by multiwavelength x-ray diffraction on the selenomethionyl protein at 2.9-A resolution. *Proc. Natl Acad. Sci. USA*, **94**, 6652–6657.
10. Raghunathan,S., Kozlov,A.G., Lohman,T.M. and Waksman,G. (2000) Structure of the DNA binding domain of E. coli SSB bound to ssDNA. *Nat. Struct. Biol.*, **7**, 648–652.
11. Yang,C., Curth,U., Urbanke,C. and Kang,C.H. (1997) Crystal structure of human mitochondrial single stranded DNA binding protein at 2.4 angstrom resolution. *Nat. Struct. Biol.*, **4**, 153–157.
12. Fanning,E., Klimovich,V. and Nager,A.R. (2006) A dynamic model for replication protein A (RPA) function in DNA processing pathways. *Nucleic Acids Res.*, **34**, 4126–4137.
13. Bernstein,D.A., Eggington,J.M., Killoran,M.P., Misic,A.M., Cox,M.M. and Keck,J.L. (2004) Crystal structure of the Deinococcus radiodurans single-stranded DNA-binding protein suggests a mechanism for coping with DNA damage. *Proc. Natl Acad. Sci. USA*, **101**, 8575–8580.
14. Dabrowski,S., Olszewski,M., Piatek,R., Brillowska-Dabrowska,A., Konopa,G. and Kur,J. (2002) Identification and characterization of single-stranded-DNA-binding proteins from Thermus thermophilus and Thermus aquaticus - new arrangement of binding domains. *Microbiology*, **148**, 3307–3315.
15. Dabrowski,S., Olszewski,M., Piatek,R. and Kur,J. (2002) Novel thermostable ssDNA-binding proteins from Thermus thermophilus and T. aquaticus-expression and purification. *Protein Expr. Purif.*, **26**, 131–138.
16. Eggington,J.M., Haruta,N., Wood,E.A. and Cox,M.M. (2004) The single-stranded DNA-binding protein of Deinococcus radiodurans. *BMC Microbiol.*, **4**, 2.
17. Fedorov,R., Witte,G., Urbanke,C., Manstein,D.J. and Curth,U. (2006) 3D structure of Thermus aquaticus single-stranded DNA-binding protein gives insight into the functioning of SSB proteins. *Nucleic Acids Res.*, **34**, 6708–6717.
18. Jedrzejczak,R., Dauter,M., Dauter,Z., Olszewski,M., Dlugolecka,A. and Kur,J. (2006) Structure of the single-stranded DNA-binding protein SSB from Thermus aquaticus. *Acta Crystallogr. D*, **62**, 1407–1412.
19. Filipkowski,P., Koziatek,M. and Kur,J. (2006) A highly thermostable, homodimeric single-stranded DNA-binding protein from Deinococcus radiopugnans. *Extremophiles*, **10**, 607–614.
20. Filipkowski,P., Duraj-Thatte,A. and Kur,J. (2006) Novel thermostable single-stranded DNA-binding protein (SSB) from Deinococcus geothermalis. *Arch. Microbiol.*, **186**, 129–137.
21. Filipkowski,P. and Kur,J. (2007) Identification and properties of the Deinococcus grandis and Deinococcus proteolyticus single-stranded DNA binding proteins (SSB). *Acta. Biochim. Pol.*, **54**, 79–87.
22. Lockhart,J.S. and DeVeaux,L.C. (2013) The essential role of the Deinococcus radiodurans ssb gene in cell survival and radiation tolerance. *PLoS One*, **8**, e71651.

23. George,N.P., Ngo,K.V., Chitteni-Pattu,S., Norais,C.A., Battista,J.R., Cox,M.M. and Keck,J.L. (2012) Structure and cellular dynamics of Deinococcus radiodurans single-stranded DNA (ssDNA)-binding protein (SSB)-DNA complexes. *J. Biol. Chem.*, **287**, 22123–22132.
24. Kozlov,A.G., Eggington,J.M., Cox,M.M. and Lohman,T.M. (2010) Binding of the dimeric Deinococcus radiodurans single-stranded DNA binding protein to single-stranded DNA. *Biochemistry*, **49**, 8266–8275.
25. Kozlov,A.G. and Lohman,T.M. (2002) Stopped-flow studies of the kinetics of single-stranded DNA binding and wrapping around the Escherichia coli SSB tetramer. *Biochemistry*, **41**, 6032–6044.
26. Roy,R., Kozlov,A.G., Lohman,T.M. and Ha,T. (2009) SSB protein diffusion on single-stranded DNA stimulates RecA filament formation. *Nature*, **461**, 1092–1097.
27. Zhou,R., Kozlov,A.G., Roy,R., Zhang,J., Korolev,S., Lohman,T.M. and Ha,T. (2011) SSB functions as a sliding platform that migrates on DNA via reptation. *Cell*, **146**, 222–232.
28. Kumaran,S., Kozlov,A.G. and Lohman,T.M. (2006) Saccharomyces cerevisiae replication protein A binds to single-stranded DNA in multiple salt-dependent modes. *Biochemistry*, **45**, 11958–11973.
29. Roy,R., Kozlov,A.G., Lohman,T.M. and Ha,T. (2007) Dynamic structural rearrangements between DNA binding modes of E. coli SSB protein. *J. Mol. Biol.*, **369**, 1244–1257.
30. Witte,G., Fedorov,R. and Curth,U. (2008) Biophysical analysis of Thermus aquaticus single-stranded DNA binding protein. *Biophys. J.*, **94**, 2269–2279.
31. Witte,G., Urbanke,C. and Curth,U. (2005) Single-stranded DNA-binding protein of Deinococcus radiodurans: a biophysical characterization. *Nucleic Acids Res.*, **33**, 1662–1670.
32. Eggington,J.M., Kozlov,A.G., Cox,M.M. and Lohman,T.M. (2006) Polar destabilization of DNA duplexes with single-stranded overhangs by the Deinococcus radiodurans SSB protein. *Biochemistry*, **45**, 14490–14502.
33. Ha,T., Enderle,T., Ogletree,D.F., Chemla,D.S., Selvin,P.R. and Weiss,S. (1996) Probing the interaction between two single molecules: Fluorescence resonance energy transfer between a single donor and a single acceptor. *Proc. Natl Acad. Sci. USA*, **93**, 6264–6268.
34. Roy,R., Hohng,S. and Ha,T. (2008) A practical guide to single-molecule FRET. *Nat. Methods*, **5**, 507–516.
35. Inoue,J., Shigemori,Y. and Mikawa,T. (2006) Improvements of rolling circle amplification (RCA) efficiency and accuracy using Thermus thermophilus SSB mutant protein. *Nucleic Acids Res.*, **34**, e69.
36. Inoue,J., Honda,M., Ikawa,S., Shibata,T. and Mikawa,T. (2008) The process of displacing the single-stranded DNA-binding protein from single-stranded DNA by RecO and RecR proteins. *Nucleic Acids Res.*, **36**, 94–109.
37. Zhou,R. and Ha,T. (2012) Single-molecule analysis of SSB dynamics on single-stranded DNA. *Methods Mol. Biol.*, **922**, 85–100.
38. Zhou,R., Kozlov,A.G., Roy,R., Zhang,J.C., Korolev,S., Lohman,T.M. and Ha,T. (2011) SSB functions as a sliding platform that migrates on DNA via reptation. *Cell*, **146**, 485–485.
39. Kim,H.D., Nienhaus,G.U., Ha,T., Orr,J.W., Williamson,J.R. and Chu,S. (2002) Mg2+-dependent conformational change of RNA studied by fluorescence correlation and FRET on immobilized single molecules. *Proc. Natl Acad. Sci. USA*, **99**, 4284–4289.
40. Murphy,M.C., Rasnik,I., Cheng,W., Lohman,T.M. and Ha,T. (2004) Probing single-stranded DNA conformational flexibility using fluorescence spectroscopy. *Biophys. J.*, **86**, 2530–2537.
41. Antony,E., Weiland,E.A., Korolev,S. and Lohman,T.M. (2012) Plasmodium falciparum SSB tetramer wraps single-stranded DNA with similar topology but opposite polarity to E. coli SSB. *J. Mol. Biol.*, **420**, 269–283.
42. Karymov,M., Daniel,D., Sankey,O.F. and Lyubchenko,Y.L. (2005) Holliday junction dynamics and branch migration: single-molecule analysis. *Proc. Natl Acad. Sci. USA*, **102**, 8186–8191.
43. Joo,C., McKinney,S.A., Lilley,D.M. and Ha,T. (2004) Exploring rare conformational species and ionic effects in DNA Holliday junctions using single-molecule spectroscopy. *J. Mol. Biol.*, **341**, 739–751.
44. Antony,E., Kozlov,A.G., Nguyen,B. and Lohman,T.M. (2012) Plasmodium falciparum SSB Tetramer Binds Single-Stranded DNA Only in a Fully Wrapped Mode. *J. Mol. Biol.*, **420**, 284–295.
45. McKinney,S.A., Joo,C. and Ha,T. (2006) Analysis of single-molecule FRET trajectories using hidden Markov modeling. *Biophys. J.*, **91**, 1941–1951.
46. Hwang,H., Buncher,N., Opresko,P.L. and Myong,S. (2012) POT1-TPP1 regulates telomeric overhang structural dynamics. *Structure*, **20**, 1872–1880.
47. Honda,M., Okuno,Y., Yoo,J., Ha,T. and Spies,M. (2011) Tyrosine phosphorylation enhances RAD52-mediated annealing by modulating its DNA binding. *EMBO J.*, **30**, 3368–3382.
48. Rothenberg,E., Grimme,J.M., Spies,M. and Ha,T. (2008) Human Rad52-mediated homology search and annealing occurs by continuous interactions between overlapping nucleoprotein complexes. *Proc. Natl Acad. Sci. USA*, **105**, 20274–20279.
49. Perales,C., Cava,F., Meijer,W.J.J. and Berenguer,J. (2003) Enhancement of DNA, cDNA synthesis and fidelity at high temperatures by a dimeric single-stranded DNA-binding protein. *Nucleic Acids Res.*, **31**, 6473–6480.
50. Kur,J., Olszewski,M., Dlugolecka,A. and Filipkowski,P. (2005) Single-stranded DNA-binding proteins (SSBs) - sources and applications in molecular biology. *Acta Biochim. Polonica*, **52**, 569–574.
51. Wessel,S.R., Marceau,A.H., Massoni,S.C., Zhou,R., Ha,T., Sandler,S.J. and Keck,J.L. (2013) PriC-mediated DNA replication restart requires PriC complex formation with the single-stranded DNA-binding protein. *J. Biol. Chem.*, **288**, 17569–17578.